J. Fluid Mech. (1990), *vol.* 212, *pp.* 615–636
Printed in Great Britain

An experimental investigation of an incompressible turbulent boundary layer in the vicinity of separation

By P. DENGEL AND H. H. FERNHOLZ
Hermann-Föttinger-Institut, Technische Universität Berlin, Strasse des 17 Juni 135, D-1000 Berlin 12

(Received 8 June 1989)

The following is an investigation into the effects of small changes in the static pressure distribution on the development of an axisymmetric, incompressible, turbulent boundary layer with incipient separation. The pressure distribution was closely controlled to study three cases, in which the skin friction was either approximately zero, slightly negative, or slightly positive along a fixed length. Mean flow and turbulence structure in air were measured using pulsed-wire and hot-wire anemometry.

These measurements show characteristic properties of steady turbulent boundary layers both on the verge of separation and with a long, shallow separation bubble. There is an asymptotic velocity defect law near separation. A linear relationship between χ_w, the wall value of the reverse-flow parameter, and the form parameter H_{12} suggests the importance of χ_w in characterizing the boundary layer. The occurrence of the first reverse-flow events coincides with the vanishing of the logarithmic law, the asymptotic mean velocity profile, and a sudden drop in the values of the skewness S_w and the flatness F_w of the skin friction. This implies that the presence of instantaneous reverse flow is associated with a complete change in the nature of the near-wall flow, well upstream of mean separation. As the three cases were investigated in a single test section under closely controlled conditions with the same experimental techniques, this data set is well suited to a sensitivity study. It is possible to show the effect of small changes in the upstream pressure gradient on the separation region and to distinguish the effect of mean reverse flow from that of the adverse pressure gradient. This effect of the reverse flow is displayed most clearly in a plateau in $\overline{u'^2}$ near the wall and in unusual behaviour of the skewness and the flatness profiles over the inner half of the boundary layer.

1. Introduction

Among the boundary conditions affecting a wall boundary layer, the pressure distribution in the main stream direction has the most important effect in the majority of practical flows. If the pressure gradient is positive, the flow will usually separate from the wall, and this is more often than not detrimental. To prevent separation and yet obtain a large pressure rise, the pressure should increase sharply where the boundary layer is thin and then flatten off as separation threatens. Prandtl (1935) appears to have been the first to solve this inverse boundary-layer problem. He calculated the pressure distribution for a laminar boundary layer which remained on the verge of separation (zero skin friction), thus allowing a maximum pressure

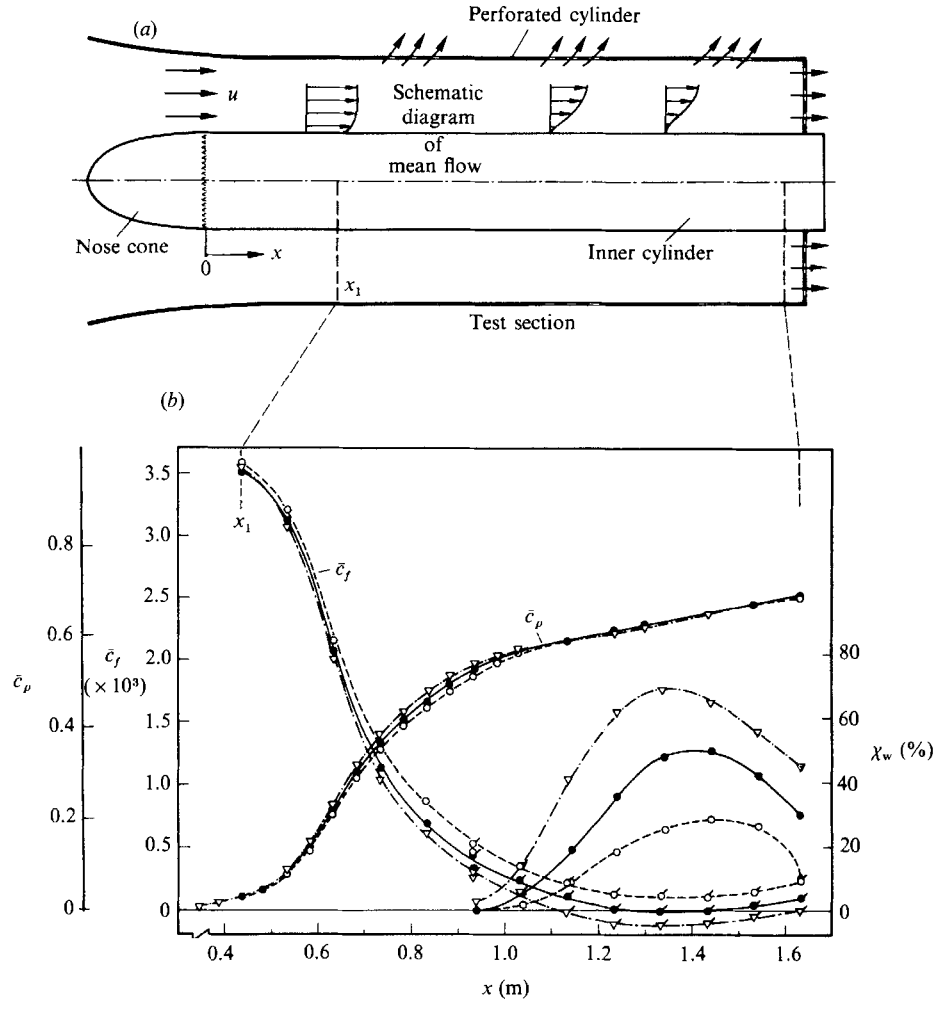

FIGURE 1. (*a*) Sketch of test facility. (*b*) Static pressure, reverse-flow parameter χ_w, and skin-friction distributions of the three test cases. Lines for visual aid only. $\bar{c}_p = (\bar{p}(x) - p(\text{ref}))/(0.5\rho u_D^2)$; $\bar{c}_f = \bar{\tau}_w/(0.5\rho u_D^2)$: ●, case 1; ○, case 2; ▽, case 3.

recovery. About twenty-five years later Stratford (1959) published the results of an experiment in which he proved that a stable turbulent boundary layer with 'near zero skin friction' could be generated. At the time, however, measurement techniques were not sophisticated enough to perform measurements either of skin friction near incipient separation or of velocity profiles with instantaneous or mean reverse flow. Prandtl's calculation was extended to turbulent boundary layers by Fernholz (1966), and further attempts at an experimental verification of such a boundary layer in axisymmetric flow configurations were reported by Fernholz (1968) and by Dengel, Fernholz & Vagt (1982). These investigations, although improvements on the earlier experiment of Stratford, still lacked adequate experimental techniques. Only the later development of the wall pulsed wire made it possible to determine accurately the occurrence of zero skin friction and thus to achieve the required pressure distribution.

Instead of studying boundary layers remaining on the verge of separation several recent workers have investigated boundary layers with large reverse-flow regions, e.g. Simpson, Chew & Shivaprasad (1981*a*), Wadcock (1985), Thompson & Whitelaw (1985), and Patrick (1987), using laser-Doppler anemometry and the flying hot-wire technique. The height of these separation regions can become comparable with the thickness of the boundary layer at separation; this leads not only to strong viscid/inviscid interaction, but also to large streamline curvature near separation, associated with normal pressure gradients (cf. Patrick 1987). It is difficult to compare these experiments directly, as the effect of these influences depends both on the incoming flow and on the bubble geometry. In addition, some but not all of these experiments indicate low-frequency unsteadiness in the separation region ('flapping'). Finally, separated flows are particularly sensitive to secondary flows, for instance corner flows originating upstream.

The present investigation examines the behaviour of boundary layers in the vicinity of separation; this work is a combination of the two types of separating flow discussed above. Three similar flows are studied, each with slightly different pressure distributions resulting in finite regions of small, constant, but different skin frictions as shown in figure 1(*b*): case 1, approximately zero; case 2, slightly positive ($c_f \sim 0.0001$); and case 3, slightly negative ($c_f \sim -0.0001$). In that the skin friction is small and constant over a fixed length, this investigation is an extension of the Prandtl/Stratford work on boundary layers on the verge of separation; this study uses modern pulsed-wire anemometry and examines the sensitivity of a boundary layer near separation to small perturbations in the streamwise pressure gradient. In addition, case 3 includes a long, shallow separation bubble, a considerably weaker version of that studied by the more recent investigations mentioned above. That the bubble is small (compared to the boundary-layer thickness) minimizes viscid/inviscid interaction and normal pressure gradients. It is steady (no flapping) and grows on an axisymmetric cylinder to prevent three-dimensional effects.

2. Experimental arrangement and measuring techniques

The wind tunnel used in this investigation (Dengel 1989) was a low-speed blower tunnel with a 12 KW motor and a centrifugal fan, an airfilter intake, and 2 m long settling chamber of circular cross-section containing, at its upstream end, a precisely manufactured, perforated metal screen (64% open area ratio), and a non-woven filter mat. The nozzle leading to the axisymmetric test section had a contraction ratio of 11:1. The core velocity distribution was uniform at the nozzle exit to within $\pm 0.3\%$, with a turbulence intensity of 0.2%. The test section (figure 1*a*) consisted of a sting-mounted, horizontal, inner circular cylinder (0.25 m diameter, 1.85 m long, and made of Ultramid S) with an elliptical nose cone (0.30 m long) extending upstream into the nozzle and thus increasing the contraction ratio to 13.4:1. The inner cylinder could be rotated through a circumferential angle of 160°. The outer cylindrical wall was concentric with the inner surface and both the outer wall and the back plate were constructed of perforated metal sheet (38% open area ratio). Despite accurate alignment of the test section, non-uniformities in the skin-friction distribution around the circumference of the inner cylinder had always been a problem and were found to be at least $\pm 8\%$ of $\bar{c}_f$ (Fernholz & Vagt 1977). These variations were reduced to $\pm 1\%$ (Dengel & Fernholz 1989) by replacing the screens in the settling chamber with one accurately manufactured, perforated metal screen and a non-woven filter mat.

The removal of the screens eliminated a main source of disturbances, disturbances which had been amplified by the test boundary layer and resulted in the 'peak-and-valley' pattern of the skin friction around the circumference.

The pressure distributions which generated the three boundary layers were set up by partially closing the open areas of the back plate and the outer cylinder. Sufficiently accurate measurements of pressure distributions can only be made if the pressure is measured with a single pressure tapping (movable in the x-direction) and not with a series of tappings along a generator of the cylinder as had been used earlier (see Dengel *et al.* 1982). Because this technique measures relative pressure levels so accurately the pressure gradients, calculated without smoothing, can be clearly distinguished between the three cases (see figure 4).

In the upstream part of the flow, the skin friction was measured by Preston tubes (symbols without a flag in figure 1*b*). Downstream, where instantaneous reverse flow occurred, the skin friction was measured by a wall pulsed-wire probe, the principle of which is discussed in Dengel, Fernholz & Hess (1987), for example. At one position ($x = 0.931$ m) measurements from a wall pulsed wire (flagged symbols) and a Preston tube are shown for comparison.

All traversing probes were mounted on an electrically driven gear and introduced into the test section through a slot along a generator of the outer cylinder wall. The traverse gear provided precise linear movements (incremental resolution 0.005 mm). Mean and fluctuating velocities were measured using a single normal-wire probe (Vagt & Fernholz 1979) and a miniature X-wire probe (cage face of 1.5×0.7 mm^2) in regions without instantaneous reverse flow, and with pulsed-wire probes everywhere else. The hot-wire anemometer system consisted of two CT bridges (IFA-100, TSI) in combination with two A/D converters (PSI) and a Commodore 3032 computer. The pulsed-wire probes were operated by a PELA-Flow Instruments anemometer, modified in-house. For details of the instrumentation, the calibration procedures, and the uncertainty estimates, the reader is referred to Dengel (1989).

The reference velocity u_D at the inlet of the test section was used to monitor the unit Reynolds number (10^6 m^{-1}, kept constant to within $\pm 10^3$ m^{-1} with a flow temperature of 21.5 ± 0.2 °C).

3. Mean flow measurements

A survey of the distribution of three important boundary-layer parameters is shown in figure 1(*b*). $\bar{c}_p$ is the pressure coefficient $(\bar{p}(x) - p(\mathrm{ref}))/(0.5\rho u_D^2)$, where $\bar{p}$ is the static pressure, p(ref) the static pressure where u_D is measured, and ρ the density; $\bar{c}_f$ is the skin-friction coefficient $(\bar{\tau}_w/(0.5\rho u_D^2))$, with $\bar{\tau}_w$ as the mean value of the skin friction; and χ_w is the wall value of the reverse-flow parameter, defined as the fraction of time the flow travels in the upstream direction, as measured by the wall pulsed-wire probe (wires 0.03 mm above the wall).

As described above, our goal was to generate three different skin-friction distributions from slight variations in the upstream pressure distribution. Although the magnitude of the skin friction in the three cases varies little, there are distinct differences in the level of the reverse-flow parameter. Cases 1 and 3 have in common, however, that skin friction zero coincides with $\chi_w = 50\,\%$, which agrees with 'transitory detachment (TD)' in the classification of Simpson *et al.* (1981*a*). This is true both at separation and at reattachment.

Figure 2 presents the mean velocity distributions for the three cases in the flow region of main interest, i.e. where the boundary layer in case 1 approaches and

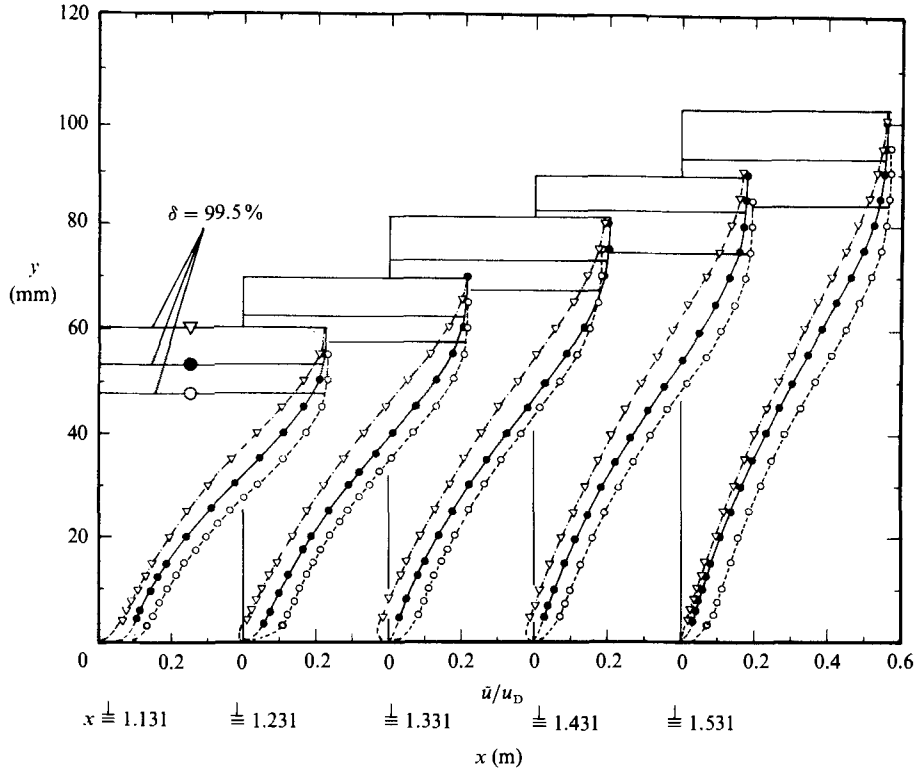

FIGURE 2. Mean velocity profiles of the three flows in the downstream region (pulsed-wire data). Symbols as in figure 1(*b*). Lines for visual aid only.

remains on the verge of separation (1.23 m $\leqslant x \leqslant$ 1.53 m). At the last station all boundary layers have positive skin friction. The mean velocity profiles show a clearly wake-like form with the inflection point far out in the flow; they are very similar despite their different skin-friction distributions.

The mean-flow profiles were used to calculate the form parameter $H_{12} = \delta_1/\delta_2$, the ratio of the displacement and momentum-loss thicknesses. For axisymmetric flow they are defined as follows:

$$\delta_1 = \left\{R^2 + 2R\int_0^{\delta}\left(1-\frac{\bar{u}(y)}{u_\delta}\right)\left(1+\frac{y}{R}\right)\mathrm{d}y\right\}^{\frac{1}{2}} - R, \tag{3.1}$$

$$\delta_2 = \left\{R^2 + 2R\int_0^{\delta}\frac{\bar{u}(y)}{u_\delta}\left(1-\frac{\bar{u}(y)}{u_\delta}\right)\left(1+\frac{y}{R}\right)\mathrm{d}y\right\}^{\frac{1}{2}} - R, \tag{3.2}$$

where R is the radius of the inner cylinder. Figure 3 displays the influence of the small variations in the static pressure gradient (figure 4) on the development of the displacement thickness (strong, approximately 30% between case 2 and 3) and the momentum-loss thickness (weak). The strong increase of δ_1 accompanies the advent of boundary-layer separation; its large growth is as much a characteristic of the approach towards separation as the decrease of $\bar{\tau}_w$ to zero. Note that the Reynolds number Re_{δ_2} increases over the length of the circular cylinder from about 4×10^3 to 11×10^3 at the downstream end, indicating a fully developed turbulent regime.

The distributions of the form parameter H_{12} are shown in figure 4. They vary by

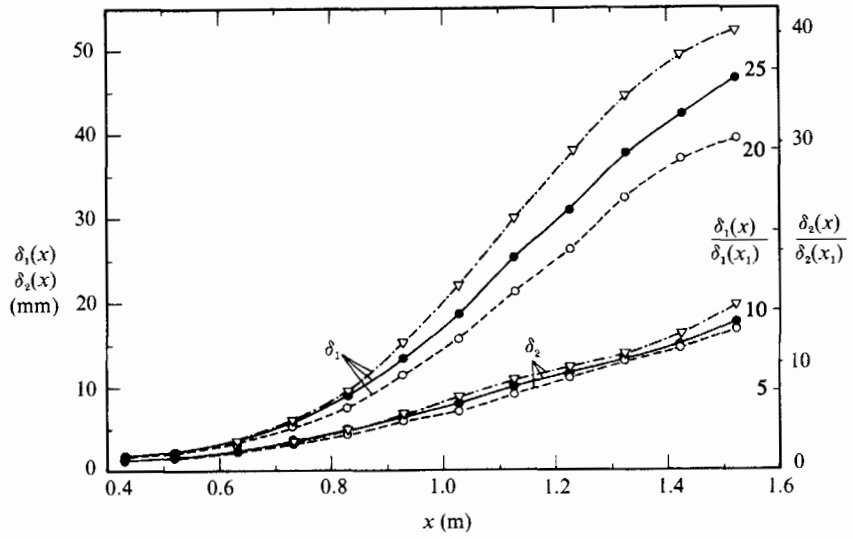

FIGURE 3. Distributions of displacement and momentum-loss thickness $\delta_1(x_1) = 1.90$ mm; $\delta_2(x_1) = 1.30$ mm. Symbols as in figure 1(*b*). Lines for visual aid only.

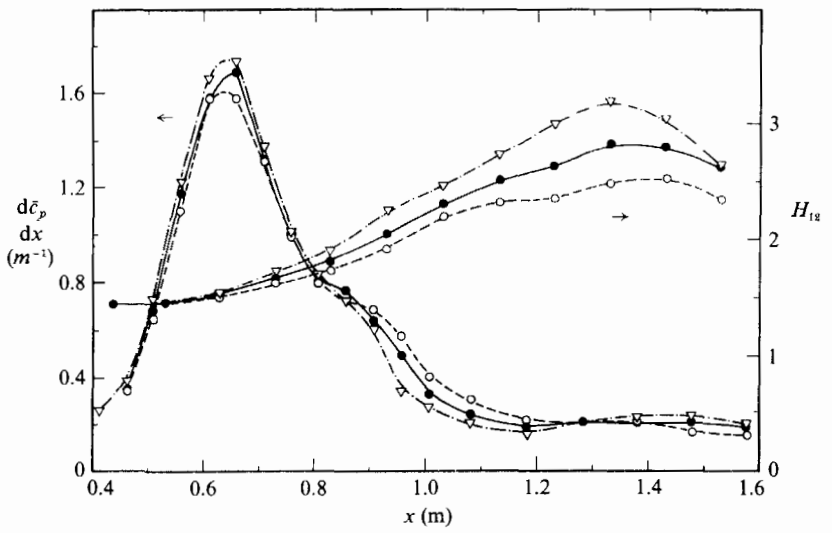

FIGURE 4. Distributions of the form parameter H_{12} and the pressure gradient $d\bar{c}_p/dx$. Symbols as in figure 1(*b*). Lines for visual aid only.

about 30% between the three cases and remain fairly constant for cases 1 and 2 in the region of interest. Since a correlation was found between the mean skin friction at separation ($\bar{\tau}_w = 0$) and the reverse-flow parameter $\chi_w = 50\%$, we also looked for a correlation between H_{12} and χ_w. Figure 5 shows all sets of (H_{12}, χ_w) in the range $0.02 \leqslant \chi_w \leqslant 0.70$ and displays an almost linear relationship for most of our data. The exceptions are those values of H_{12} measured where the skin-friction gradient becomes positive (symbols denoted by a flag). For $\chi_w = 50\%$ the corresponding value of H_{12} is $2.85 \pm 0.1\%$. We claim that this value is characteristic of transitory detachment for separating boundary layers of the present type. However, it may be affected by Reynolds number, high free-stream turbulence, large bubble size, etc.

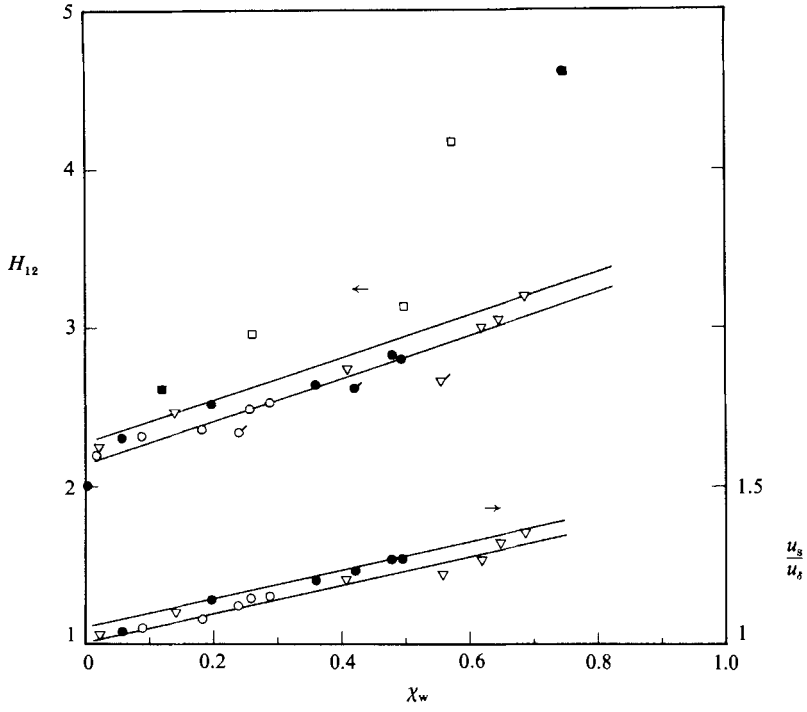

FIGURE 5. Relationship between form parameter H_{12}, Perry–Schofield-velocity scale, and reverse-flow parameter. ●, ○, ▽, cases 1, 2, and 3, respectively. ■, □, Simpson *et al.* (1977, 1981*a*).

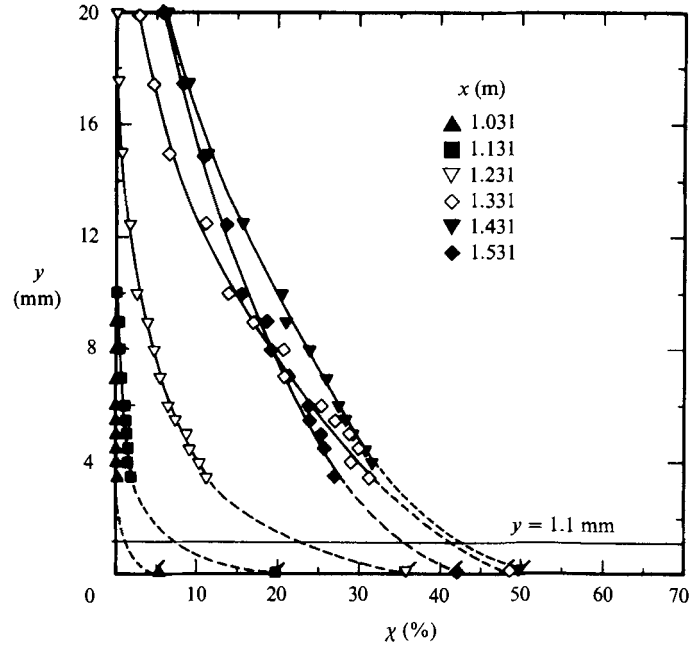

FIGURE 6. Profiles of the reverse-flow parameter χ at various x-stations (case 1). Lines for visual aid only.

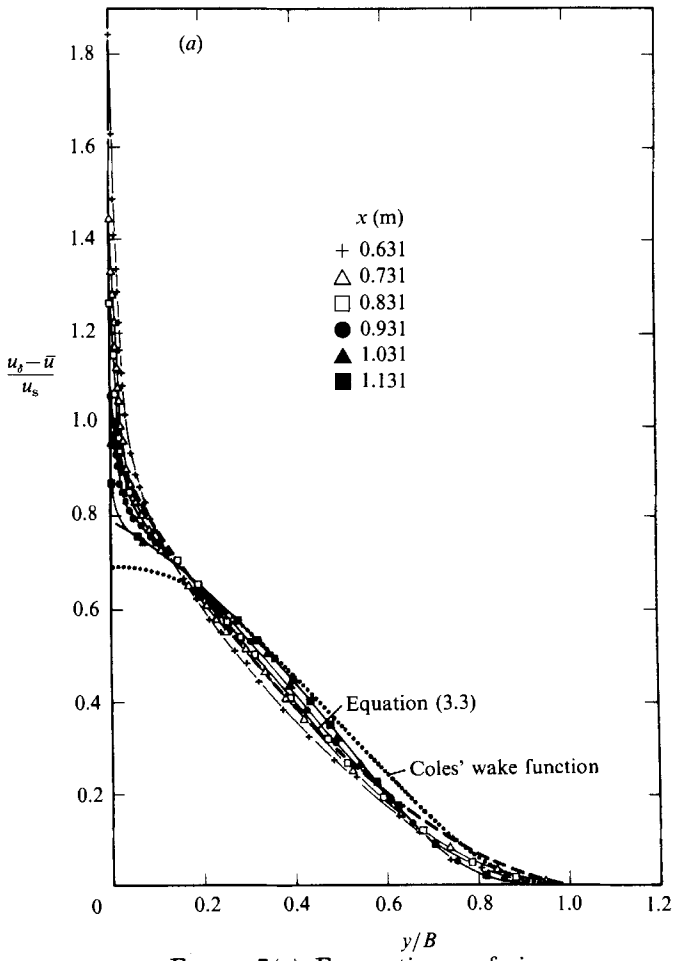

FIGURE 7(*a*). For caption see facing page.

A comparison with the results of other investigations of separated flow is problematic for the reasons discussed in the introduction. Furthermore, χ_w measurements are rare and difficult to perform accurately. Figure 5 includes the only other (H_{12}, χ_w) data available, from Simpson, Strickland & Barr (1977) and Simpson *et al.* (1981*a*); these results do not show the same linear relationship as the present data. However, χ is a strong function of the distance from the wall, so that χ_w measurements depend on the size of the probe used. This is illustrated in figure 6, showing several χ-profiles measured with a traversing pulsed wire; the data points are extrapolated to the wall value as measured by a wall pulsed wire with sensor wires 0.03 mm above the wall. Simpson's *et al.* 'χ_w' was measured 1.1 mm above the surface and the figure shows, for example, that at $x = 1.53$ m χ_w is 20% larger than the extrapolated value 1.1 mm above the wall. The exact relationship between χ_w and $\chi(y)$ depends, of course, on the details of the flow field, so that Simpson's *et al.* data for $\chi(y = 1.1$ mm) cannot validly be extrapolated to χ_w to be compared with our data. More importantly, a systematic error in determining χ_w leads to an erroneous determination of the position of transitory detachment and of the characteristic boundary-layer parameters at this location.

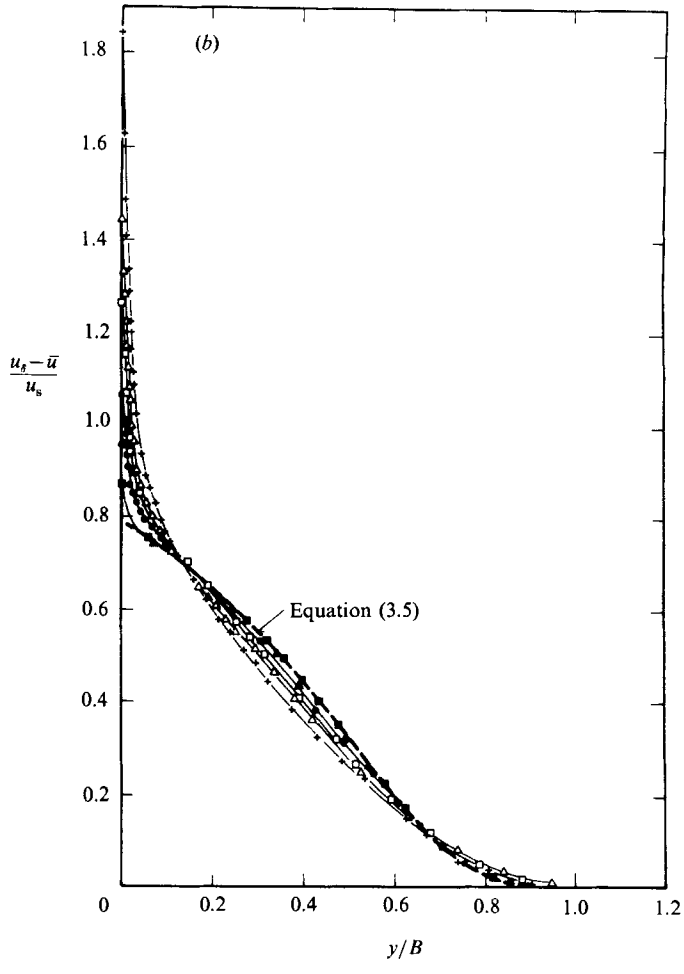

FIGURE 7 (*a*, *b*). Mean velocity profiles in Perry–Schofield coordinates. Lines for visual aid only.

Theoretical predictions of the form parameter H_{12} at separation using Coles' law of the wake resulted in values of about four (e.g. Coles 1956 and Rotta 1962), independent of the momentum-thickness Reynolds number Re_{δ_2}. Fernholz (1968) noted that Coles' law of the wake did not agree with measurements near separation, and later Perry & Schofield (1973) and Schofield (1986) attempted to establish a general defect law for adverse pressure gradient boundary layers near separation by replacing the skin-friction velocity u_τ with a scaling velocity u_s based on a half-power profile. This resulted in a defect law

$$\frac{u_\delta - \bar{u}}{u_s} = 1 - 0.4\left(\frac{y}{B}\right)^{\frac{1}{2}} - 0.6\sin\left(\frac{\pi}{2}\frac{y}{B}\right) \tag{3.3}$$

with $B = 2.86\ \delta_1 u_\delta / u_s$, and an inner law

$$\frac{\bar{u}}{u_\delta} = 0.47\left(\frac{u_s}{u_\delta}\right)^{\frac{3}{2}}\left(\frac{y}{\delta_1}\right)^{\frac{1}{2}} + 1 - \frac{u_s}{u_\delta}. \tag{3.4}$$

The velocity ratio u_s/u_δ can be determined from a measured velocity profile in a way

similar to finding u_τ/u_δ from a Clauser chart using (3.4). Schofield claimed that the profile represented by (3.3) and (3.4) applied to all adverse pressure gradient boundary layers, in equilibrium or not, with the restriction that the ratio $|\overline{u'v'}|/u_\tau^2$ must exceed 1.5.

Our measurements (an example is given in figure 7*a*) did not confirm Schofield's results. The profile he proposes is valid at only one point in adverse pressure gradient boundary layers on the way to separation and is not a particularly good approximation for the other profiles. For further comparisons see Schofield (1986) and Dengel (1989). Nevertheless Perry–Schofield coordinates are useful. In these coordinates the profiles do reach an asymptotic velocity profile but only in the vicinity of separation, and not that given by (3.3). The approach is displayed in figure 7(*b*) by profiles of case 1. Figure 8 shows the asymptotic profile which describes the boundary-layer shape for all three cases when $H_{12} \geqslant 2.2$. The upper limit on H_{12} is at least 3.2, the highest value measured in this experiment (case 3); it may be higher, but the next available data point has $H_{12} = 4.4$ (Simpson *et al.*) and it does not fall on this profile. Note that the asymptotic profile includes the profile at transitory detachment ($H_{12} = 2.85$) and that the outer 95% of these profiles are independent of the near-wall condition of the boundary layer (zero, negative, or positive skin friction). Other measurements in adverse pressure gradient boundary layers confirmed this asymptotic behaviour (e.g. Spangenberg, Rowland & Mease 1967, case B; East, Nash & Sawyer 1979, case 7; and Simpson *et al.* (1981); see again Dengel 1989).

The asymptotic distribution of this outer-law mean velocity profile can be approximated in Perry–Schofield-coordinates by the 7th-order polynomial

$$\frac{u_\delta - \bar{u}}{u_s} = \sum_{i=0}^{7} A_i \left(\frac{y}{B}\right)^i, \quad 0.025 \leqslant y/B \leqslant 0.92, \tag{3.5}$$

with the following constants:

$$A_0 = 0.781; \quad A_1 = -0.535; \quad A_2 = -0.739; \quad A_3 = -2.352;$$
$$A_4 = 13.81\ ; \quad A_5 = -33.178; \quad A_6 = -36.502; \quad A_7 = -14.324.$$

Coles' law-of-the-wall/law-of-the-wake approach is frequently used in the computation of adverse pressure gradient boundary layers, and the wake function w alone is assumed to describe the boundary-layer shape at separation ($u_\tau = 0$). As shown in figure 7(*a*), Coles' wake function is not a particularly accurate representation of this shape, which is better described by (3.5). Recasting this equation and noting that $B \approx \delta$, we can define an improved wake function w^*

$$w^*\left(\frac{y}{\delta}\right) = \begin{cases} K \sum_{i=1}^{7} B_i \left(\frac{y}{\delta}\right)^i, & 0 \leqslant \frac{y}{\delta} \leqslant 0.92 \\ 2, & 0.92 < \frac{y}{\delta} \leqslant 1, \end{cases} \tag{3.6}$$

where $B_i = -A_i$ and $K = 2.5608$, chosen to scale the curve properly. Using this new wake function, Coles' wall/wake formulation describes the mean velocity profile of boundary layers approaching separation, $2.0 \leqslant H_{12} \leqslant 2.2$. In the vicinity of separation, $2.2 \leqslant H_{12} \leqslant 3.2$, the logarithmic region becomes vanishingly small and (3.5) should be used instead of the wall/wake relationship.

Schofield (1986) attempted to relate the scaling velocity u_s to the maximum Reynolds shear stress in the profile. Our results did not confirm the correlation he

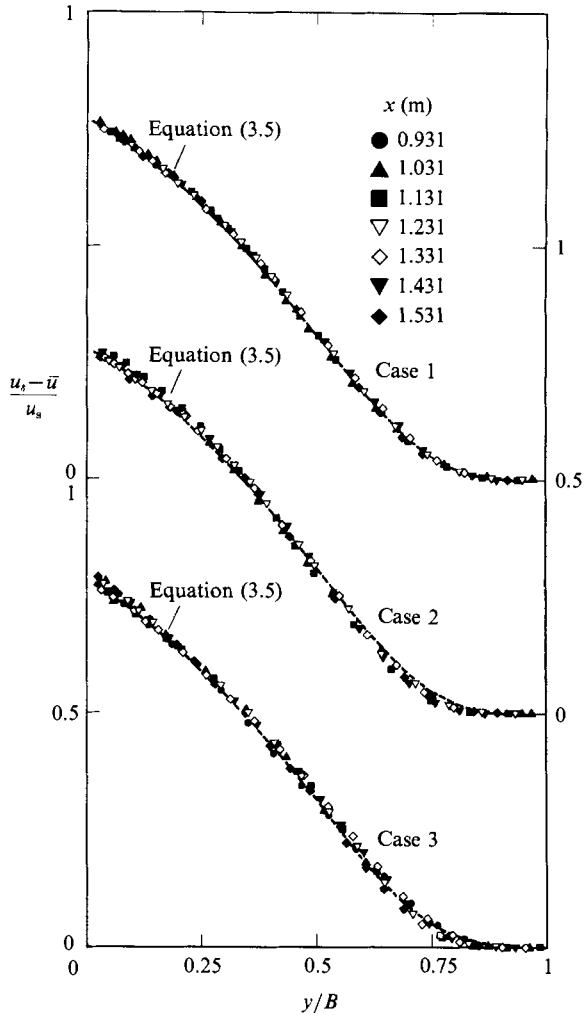

FIGURE 8. Asymptotic mean velocity profiles in Perry–Schofield coordinates.

suggested. Interestingly enough, however, we found that to a good approximation u_s/u_δ and χ_w are linearly related and may be approximated by

$$u_s/u_\delta \approx 1.01 + 0.485\chi_w \tag{3.7}$$

in the range $1\% < \chi_w < 70\%$ (see figure 5). If χ_w is known, this relationship can be used to determine u_s/u_δ as a check on the value obtained from the velocity profile.

4. Turbulence measurements

One of our goals was to measure all components of the Reynolds normal stresses and the Reynolds shear stress in and close to the separation region. It was possible to determine $\overline{u'^2}$ and $|\overline{u'v'}|$ with an uncertainty below 8% and 20%, respectively, but owing to (as yet unresolved) difficulties with the pulsed-wire probes the uncertainty in the pulsed-wire measurements of $\overline{v'^2}$ and $\overline{w'^2}$ was about 30%; these measurements

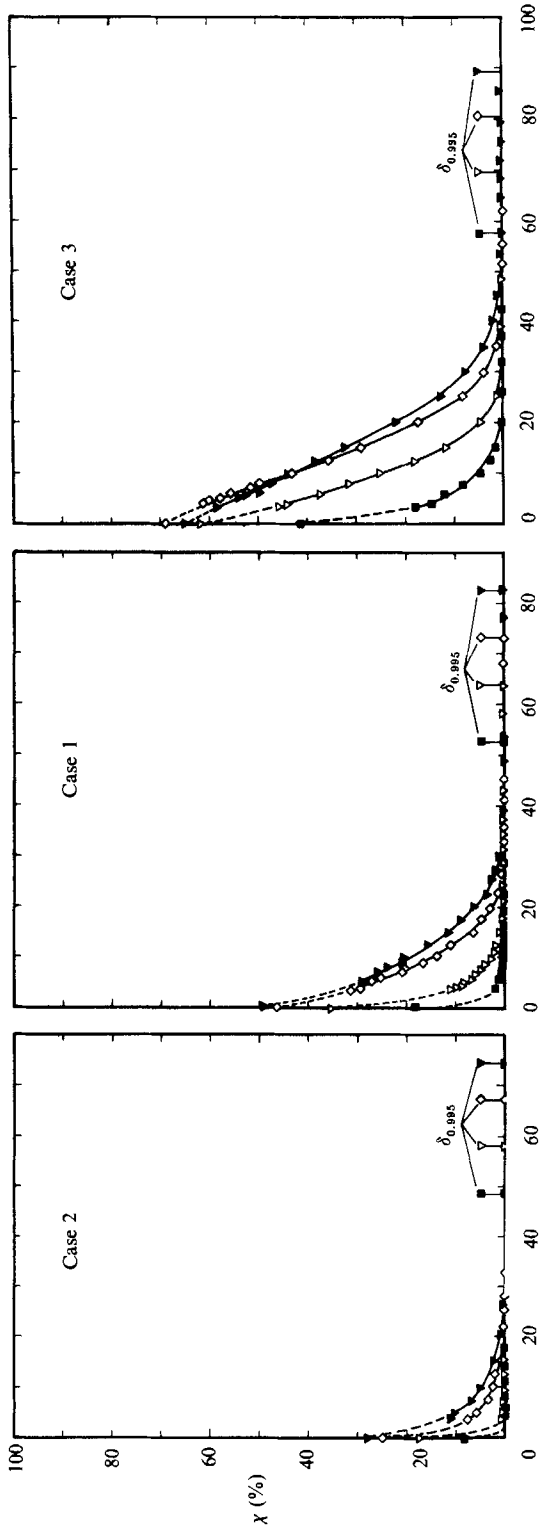

FIGURE 9. Profiles of the reverse-flow parameter χ. Symbols as in figure 6. Lines for visual aid only.

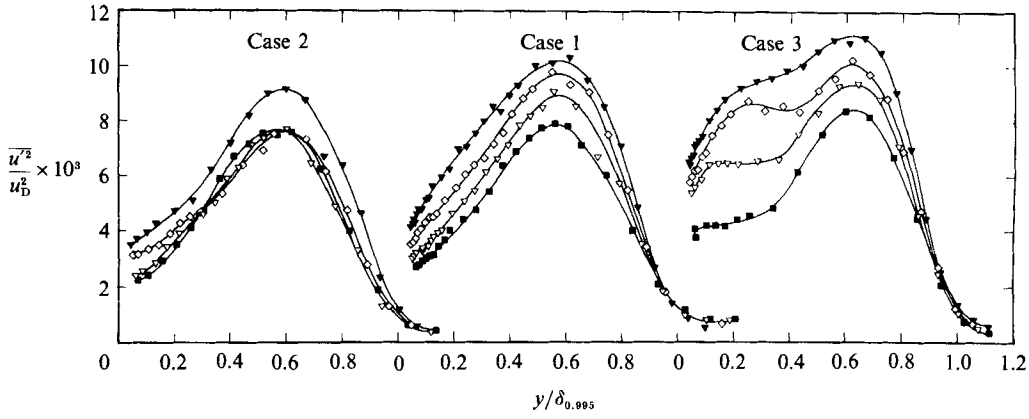

FIGURE 10. Profiles of the streamwise component of the Reynolds normal stress $\overline{u'^2}$. Symbols as in figure 6. Lines for visual aid only.

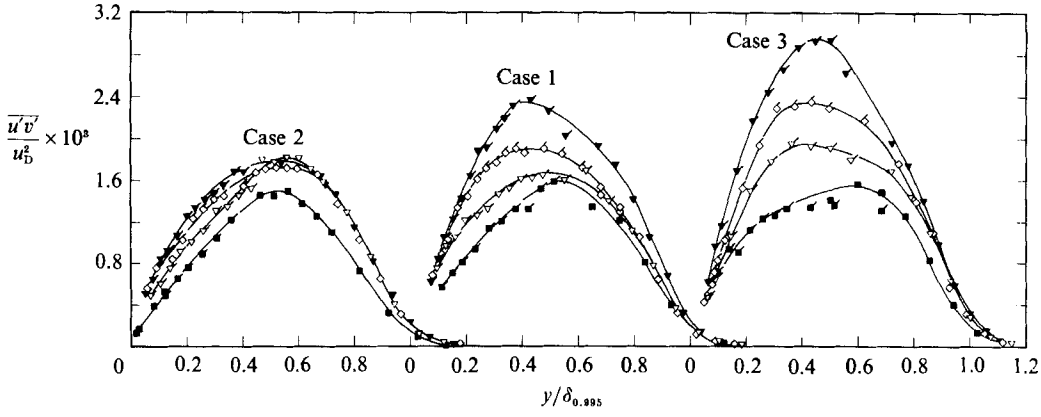

FIGURE 11. Profiles of the Reynolds shear stress. Symbols as in figure 6. Lines for visual aid only.

are therefore not discussed here. Pulsed wires were used where necessary (depending on the χ-distribution and the turbulence level) and hot wires where possible (for details see Dengel 1989). The reverse-flow parameter χ may be calculated from instantaneous velocity measurements.

Figure 9 presents profiles of the reverse-flow parameter χ in the region of main interest (1.13 m $\leqslant x \leqslant$ 1.43 m). For clarification the position of δ (always $\delta_{0.995}$) and the wall value χ_w (cf. figure 1*b*) are given. Instantaneous flow reversal for case 1, for example, begins at $x = 0.93$ m at the wall ($\chi_w = 0.35\,\%$) and spreads outward to about 8 mm (0.15δ) at $x = 1.13$ m and to 35 mm (0.43δ) at 1.43 m. As expected, the instantaneous reverse-flow region is largest in case 3 (with the shallow bubble) and smallest in case 2 (where the mean skin friction remains positive).

Figures 10 and 11 display the profiles of $(\overline{u'^2}/u_D^2)$ and $(|\overline{u'v'}|/u_D^2)$. The profiles measured for the three pressure distributions show remarkably similar shapes between the three cases except for the profile of $\overline{u'^2}$ in case 3, where a plateau appears in the wall region. While the shapes are similar, it is not possible to convert these turbulence profiles to a self-similar or asymptotic form using u_s or u_δ. The sensitivity of the $\overline{u'^2}$- and the $|\overline{u'v'}|$-profiles of cases 1 and 3 to the small changes in the pressure

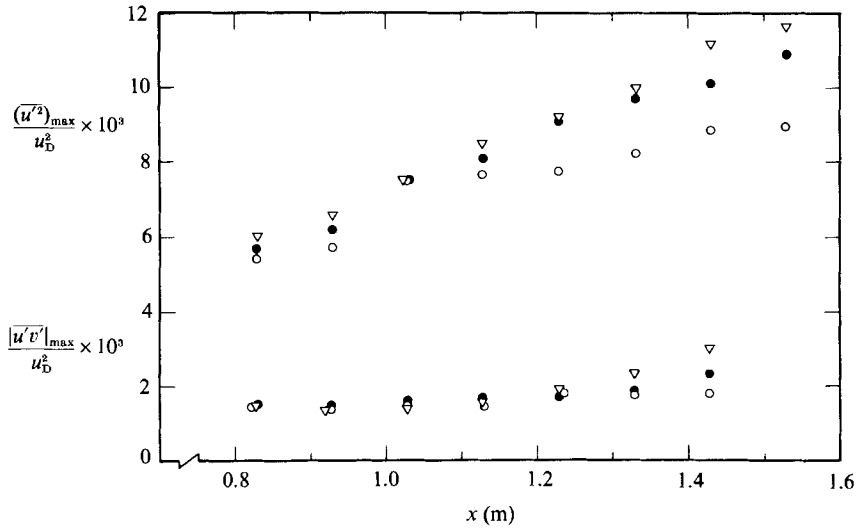

FIGURE 12. Streamwise growth in the maximum values of $\overline{u'^2}$ and $|\overline{u'v'}|$. Symbols as in figure 1(*b*).

distribution is clearly visible, and the reproduction of these profiles by a calculation method would be a good test for the sensitivity of any calculation.

Qualitatively, a similar behaviour was observed for the $\overline{v'^2}$ and $\overline{w'^2}$ profiles discussed by Dengel (1989).

Figure 12 presents the development of $(\overline{u'^2})_{max}$ and $|\overline{u'v'}|_{max}$ for the three cases. They differ in the rate of growth and in the sensitivity to the variations of the pressure distribution. $\overline{u'^2}$ is both more strongly affected by the adverse pressure gradient (approximately doubling over the range shown) and more sensitive to the differences in the three upstream pressure distributions (30% difference between cases 1 and 3). $|\overline{u'v'}|_{max}$ remains fairly constant over most of the flow, and the uncertainty in measuring $\overline{u'v'}$ obscures the differences between the three cases. By the last station, however, $\overline{u'v'}_{max}$ has grown significantly from the upstream level, and the different pressure histories are clearly reflected in the different peak shear-stress values.

Figure 13 shows that the loci of these maxima move away from the wall. This behaviour may be explained qualitatively by considering the production terms in the transport equations for $\overline{u'^2}$ and $|\overline{u'v'}|$. Without taking into account the additional second-order terms which may become important close to separation (e.g. Simpson *et al.* 1981*a*, *b*), the production terms are $|\overline{u'v'}|\,\partial\bar{u}/\partial y$ and $\overline{v'^2}\,\partial\bar{u}/\partial y$, respectively. Profiles for case 1 are presented in figure 14. In contrast to zero pressure gradient boundary layers where production peaks very close to the wall, both production terms in an adverse pressure gradient boundary layer are strongly suppressed near the wall and peak, instead, in the middle of the boundary layer. Cases 2 and 3 behave similarly.

Figure 15 compares the loci of the maxima of the Reynolds stress with those of the production maxima for case 1. Initially, there is a monotonic growth of the loci with streamwise position. This accompanies the movement away from the wall of a new local maximum in the mean velocity gradient $\partial\bar{u}/\partial y$. Farther downstream the loci reach a plateau of about 0.55δ, and the local maximum of $\partial\bar{u}/\partial y$ also remains fixed, although at approximately 0.62δ. The loci of the four quantities lie close together

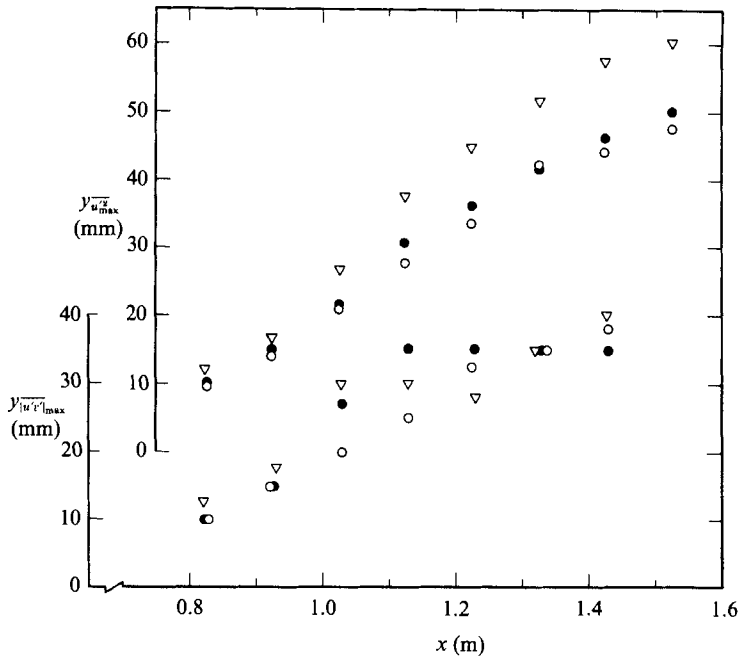

FIGURE 13. Position of the maximum of $\overline{u'^2}$ and $|\overline{u'v'}|$. Symbols as in figure 1(*b*).

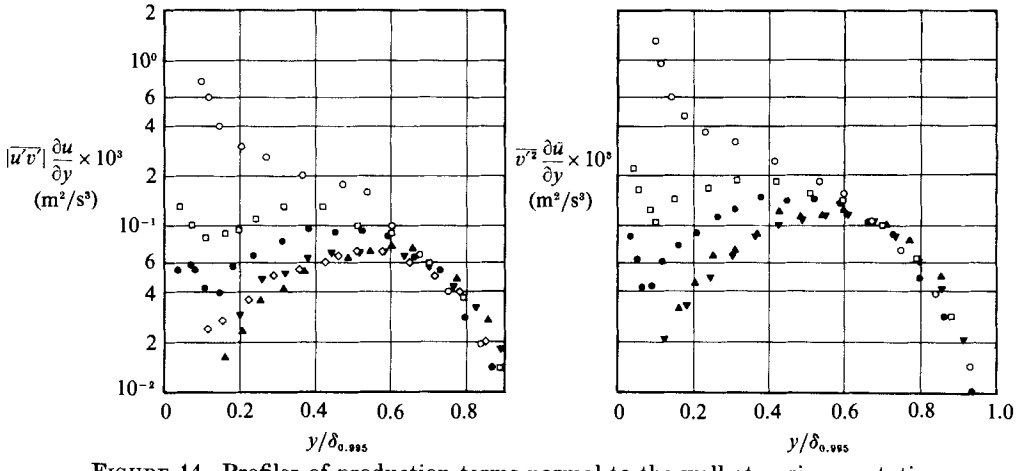

FIGURE 14. Profiles of production terms normal to the wall at various x-stations. Symbols as in figures 6 and 7 (case 1).

along the whole streamwise distance except at the last two stations, where $y_{|\overline{u'v'}|_{max}}$ decreases from the plateau. We think these data points describe the genuine behaviour of the flow but we cannot rule out a measurement error.

The production terms could have been plotted in dimensionless form (e.g. East *et al.* 1979); however, the dimensional form used in figure 14 shows the change in the absolute level of the production. Integration of the curves shows that production across the boundary layer (e.g. $\int_0^\delta |\overline{u'v'}|\,(\partial\bar{u}/\partial y)\,dy$) initially decreases as the Reynolds stresses near the wall are suppressed, but eventually increases again as the boundary layer thickens.

Further insight into the turbulence structure around the separation region may be

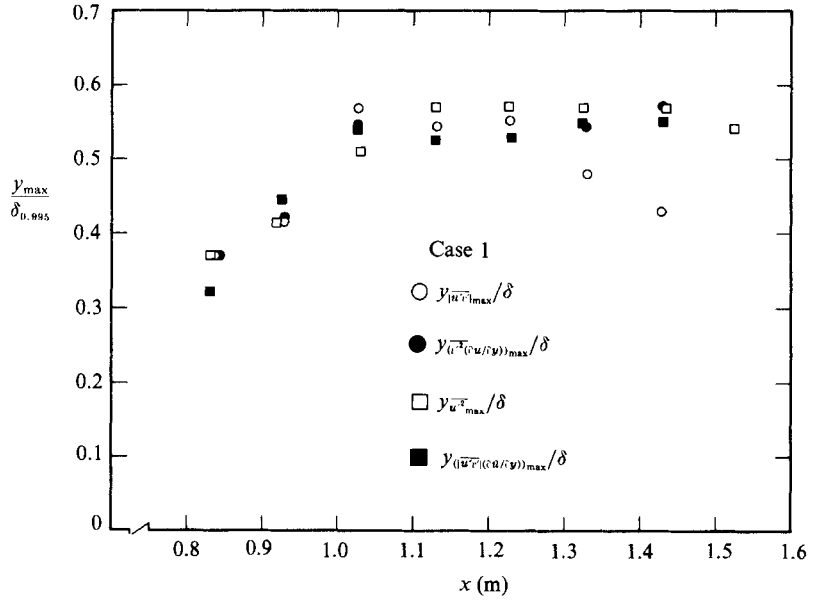

FIGURE 15. Loci of the maxima of $(\overline{u'^2})_{max}$ and $|\overline{u'v'}|_{max}$ and their production terms.

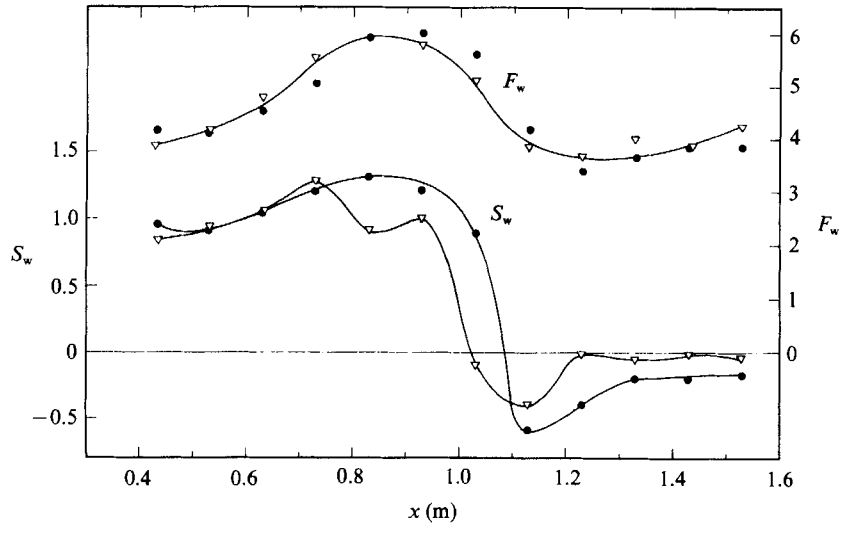

FIGURE 16. Skewness S_w and flatness F_w of the wall shear stress. Symbols as in figure 1(*b*). Lines for visual aid only.

gained from higher moments of the turbulence quantities. Figure 16 presents the skewness S_w and flatness F_w,

$$S_w = \frac{\overline{\tau_w'^3}}{(\overline{\tau_w'^2})^{\frac{3}{2}}}, \quad F_w = \frac{\overline{\tau_w'^4}}{(\overline{\tau_w'^2})^2}, \tag{4.1}$$

of the fluctuating skin friction τ_w' as measured by the wall pulsed-wire probe for cases 1 and 3. The behaviour of case 2 is similar to that of case 1 and is not discussed separately here. In the limit $y \to 0$, the instantaneous shear stress is linearly related

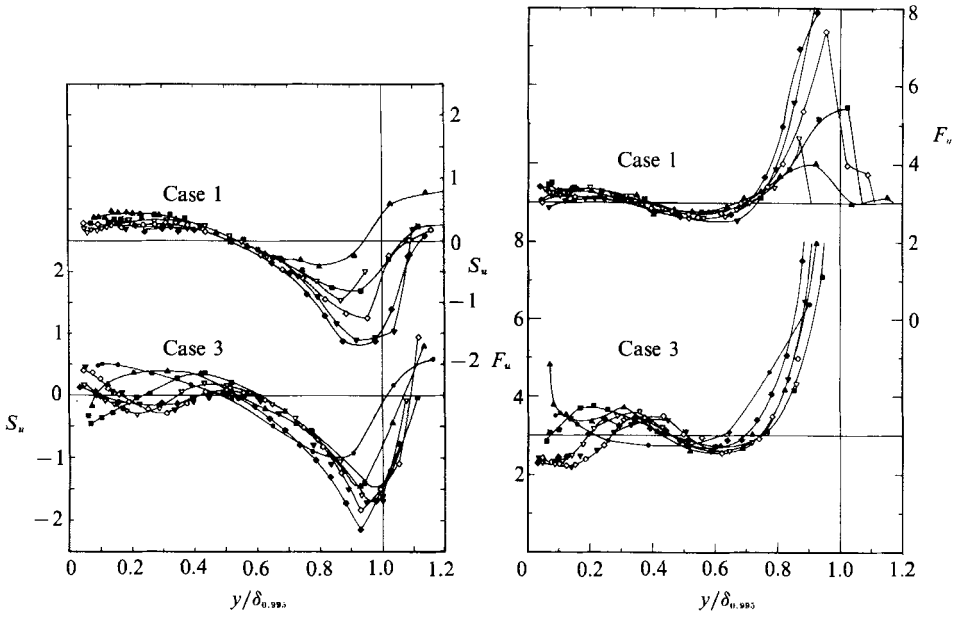

FIGURE 17. Skewness and flatness profiles of the streamwise velocity component. Symbols as in figures 6 and 7. Lines for visual aid only.

to the local velocity field, so S_w and F_w give information about the near-wall fluctuations. S_w and F_w show qualitatively similar patterns for the two flow configurations, with large positive deviations from the Gaussian behaviour ($S_w = 0$ and $F_w = 3$) in the adverse pressure gradient region (deviations similar to those found in zero pressure gradient flow), a sharp decrease to a minimum and a subsequent gradual rise towards $S_w = 0$ and $F_w = 4$. The decrease in S_w and F_w coincides with the onset of instantaneous reverse flow, $\chi_w > 0$. Johansson & Alfredsson (1982) showed that near the wall in channel flow a positive skewness reflects the presence of high shear events imposed on a background of lower turbulence level, also indicated by the high values of the flatness factor. Thus, the decrease of S_w and F_w towards separation could indicate a reduction in the frequency of high-amplitude bursts and a disappearance of this dual nature. This interpretation is consistent with the observation that production moves away from the wall.

Figure 17 displays profiles of the skewness S_u and the flatness F_u of the streamwise velocity fluctuation u' for cases 1 and 3. In the outer half of the boundary layer the skewness and flatness profiles for cases 1 and 3 are qualitatively similar and characteristic of zero pressure gradient (e.g. Andreopoulos *et al.* 1984) and adverse pressure gradient boundary layers (Simpson *et al.* 1981*b*). In both cases the skewness changes from positive to negative between 0.5δ and 0.6δ and reaches a minimum near the outer edge of the boundary layer; $S_u(y/\delta > 0.6)$ decreases in the streamwise direction. The sharp increase of the flatness with y is characteristic of the intermittent outer part of the boundary layer. The change in sign in skewness coincides in both flows with a dip in the flatness profiles and with the maxima of $\overline{u'^2}$ and its production term $\{|\overline{u'v'}|\,\partial\bar{u}/\partial y\}_{\max}$ (figure 15), as is the case near the wall in zero pressure gradient boundary layers.

In the inner half of the boundary layer, the different skin-friction histories of cases 1 and 3 are reflected in the behaviour of S_u and F_u. For case 1 the skewness profiles

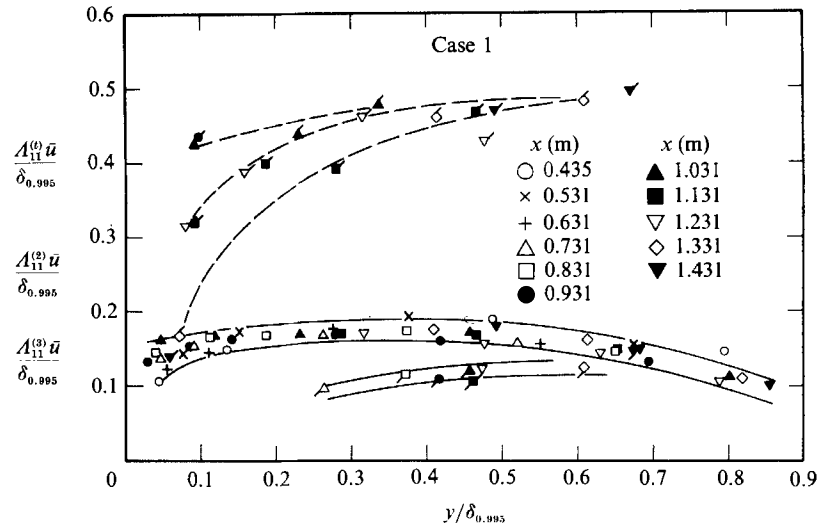

FIGURE 18. Integral lengthscales $\Lambda_x = \Lambda_{11}^{(t)}\bar{u}$, Λ_y and Λ_z in the normal direction to the wall at various positions x. Lines for visual aid only.

are fairly flat and slightly positive. The flatness is close to three for $y/\delta < 0.5$, and S_u and F_u together imply that the velocity fluctuations are Gaussian-like in the inner half of the boundary layer. Again similar results are seen in this region in zero pressure gradient boundary layers.

In case 3 (negative skin friction), the skewness and flatness behave differently in the inner half of the boundary layer. The last three profiles upstream of the separation bubble show dramatic changes in the shape of the skewness and flatness. Within the separation region the profile shapes are somewhat alike, although not self-similar. In addition to the region $S_u = 0$ near the boundary-layer centre (discussed above), S_u changes sign closer to the wall, and the flatness simultaneously reaches a minimum here. Surprisingly, the $\overline{u'^2}$-profiles (figure 10) show also local maxima or plateaux where $S_u = 0$, even though the $|\overline{u'v'}|\,\partial\bar{u}/\partial y$ production terms do not have a local maximum there.

Finally, we conclude this section with a discussion of integral lengthscales based on the longitudinal velocity fluctuation. Figure 18 shows several profiles of Λ_x, Λ_y, and Λ_z for case 1. Λ_y and Λ_z were obtained by integrating the two-point correlation functions

$$R_{11}^{(2)}(\Delta y) = \frac{\overline{u'(y)\,u'(y+\Delta y)}}{(\overline{u'^2(y)}\;\overline{u'^2(y+\Delta y)})^{\frac{1}{2}}}, \quad R_{11}^{(3)}(\Delta z) = \frac{\overline{u'(z)\,u'(z+\Delta z)}}{(\overline{u'^2(z)}\;\overline{u'^2(z+\Delta z)})^{\frac{1}{2}}}$$

to the first zero-crossing, where Δy and Δz indicate the direction of both probe separation and integration. To avoid probe interference, Λ_x was calculated by integrating the autocorrelation and using Taylor's hypothesis to convert the resulting timescale $\Lambda_{11}^{(t)}$ to a lengthscale Λ_x. Of course the use of Taylor's hypothesis is problematic in reversing flow; however, the substitution of another, more physically appropriate velocity for $\bar{u}$ does not substantially alter the conclusions drawn here.

Λ_y/δ and Λ_z/δ remain fairly constant across the layer at 0.15 and 0.1, respectively. Λ_x/δ is approximately 0.45 in the outer half of the layer and falls off near the wall. These results imply the presence of large-scale, energy-containing structures which

are three times as long as they are high (y-direction) and wide (z-direction). The integral lengthscales for cases 2 and 3 show similar behaviour (cf. Dengel 1989). The most important conclusion is that the large-scale structures in these perturbed boundary layers all scale with the boundary-layer thickness.

5. Discussion

In the following we discuss these results from several viewpoints. First we address the topic of boundary-layer behaviour in adverse pressure gradients. Next we characterize the boundary layer at and very close to separation. Finally we compare and contrast the three cases to study the sensitivity of boundary layers to small changes in pressure gradient and to small regions of mean reverse flow.

Many of our results are characteristic of adverse pressure gradient boundary layers. Increasing pressure causes a decrease in skin friction. The boundary-layer and displacement-thickness growth rates increase more strongly than that of the momentum-loss thickness, causing the mean velocity profile to lose fullness. At the wall, the decrease in the mean velocity gradient $\partial\bar{u}/\partial y$ is accompanied by a decrease in the Reynolds stresses and their production. At the same time a new local maximum of $\partial\bar{u}/\partial y$ moves away from the wall, as do the maximum Reynolds stresses and the production; however, these maxima no longer necessarily coincide. The flatness and skewness profiles in the outer half of the boundary layer look much the same as in zero pressure gradient flows.

In adverse pressure gradient flows of sufficient strength and duration, instantaneous reverse flows occurs. In the cases studied here, profiles of the reverse-flow parameter χ have steep gradients $\partial\chi/\partial y$ near the wall. In all three cases we found the same linear relationship between the wall value χ_w and the form parameter H_{12}, suggesting that χ_w is important in characterizing the boundary layer. χ_w becomes non-zero well upstream of the location of mean separation, and further indication of its importance is the observation that the first reverse-flow events occur where the log law vanishes, where the asymptotic mean velocity profile (equation (3.5)) appears, and where S_w and F_w drop suddenly. This implies that the presence of instantaneous reverse flow is associated with a complete change in the nature of the near-wall flow, even well upstream of mean separation.

In general a boundary layer changes its shape continuously in the presence of an adverse pressure gradient. Thus Schofield's attempt to find a universal profile to characterize all adverse pressure gradient boundary layers is probably futile if a high degree of accuracy is desired. However, very close to separation a universal profile does exist for the outer 95% of the boundary layer, as given by (3.5). It is valid at least in the range $2.2 \leqslant H_{12} \leqslant 3.2$; the upper limit may be slightly higher but is certainly less than 4.4. Separation itself ('transitory detachment', using Simpson's notation) is characterized by $\bar{\tau}_w = 0$, $\chi_w = 50\%$, $H_{12} = 2.85 \pm 0.1$, and $u_s/u_\delta = 1.25$. Other investigations have arrived at other values; for instance, Schofield (1986) suggested $H_{12} = 3.3$ and $u_s/u_\delta = 1.20$. However, his results were partially based on Simpson *et al.*'s measurements which, as discussed earlier, mis-identified the location of transitory detachment.

In contrast to the self-similar velocity profile near separation, the turbulence profiles do not have a universal or asymptotic form. In general the stress levels rise with x throughout the region studied here. To give a comparison with the results of other investigations, table 1 presents maximum Reynolds stresses as close to separation as measured. These data provide an impression of the magnitude of the

Author	$\left(\frac{\overline{u'^2}}{u_\delta^2}\right)_{max} \times 10^3$	$\left(\frac{\overline{\lvert u'v'\rvert}}{u_\delta^2}\right)_{max} \times 10^3$	$\left(\frac{\overline{v'^2}}{u_\delta^2}\right)_{max} \times 10^3$	$\left(\frac{\overline{w'^2}}{u_\delta^2}\right)_{max} \times 10^3$	Measuring techniques
Simpson *et al.* (1977)	18 <–< 27	3 <–< 4	4 <–< 5	12 <–< 21	LDA/HF
Wadcock (1979)	32	8	6.0	—	FHW
Shiloh *et al.* (1981)	15 <–< 25	4	4 <–< 7	4 <–< 7	LDA
Dengel *et al.* (1982)	26	—	—	—	PW
Thompson & Whitelaw (1985)	≈ 11	2	3 <–< 4	5 <–< 7	FHW
Patrick (1987)	≈ 40	—	6	—	LDA
Present experiment	23 <–< 25	4 <–< 5	9	—	PW

TABLE 1. Comparisons of maximum Reynolds stress levels close to separation, measured by various investigations (PW, pulsed-wire anemometry; LDA, laser-Doppler anemometry; FHW, flying hot wire; and HF hot film)

Reynolds stresses which can occur in separating flows and show the high degree of anisotropy present; they also illustrate the dispartity between the results of different workers. As long as there is no systematic investigation of the effects of bubble size, flapping, secondary flows, etc. it will be impossible to explain the causes of the differences.

As the measurements for our three cases were made in a single test section under closely controlled conditions with the same experimental techniques, this data set is well-suited to a sensitivity study. Not only can we show the effect of small changes in the upstream pressure gradient on the separation region (in which region the pressure distribution for all the cases is the same); we can also distinguish the effect of mean reverse flow *per se* from that of the adverse pressure gradient.

Not surprisingly, the amount of reverse flow, the increase in form parameter, and the decrease in total kinetic energy near the wall ($\bar{u}^2+\overline{q^2}$) are all continuous functions of the upstream pressure gradient: the stronger the gradient, the more χ and H_{12} increase and the more the near-wall momentum decreases. More interesting is the way the presence of mean reverse flow changes the nature of the turbulent fluctuations. This is shown most clearly in the plateau $\overline{u'^2}$ near the wall that is only present in case 3 (figure 10). It can also be seen in the unusual behaviour of the skewness and flatness profiles in case 3 over the inner half of the boundary layer (figure 17) and shows that the higher moments of u' are sensitive to mean reverse flow. Curiously, the coincidence of $\overline{u'^2_{max}}$, $S_u = 0$, and $F_{u,min}$ observed in zero pressure gradient boundary layers is preserved even above a separation bubble.

Finally, we direct a few comments towards those interested in computing boundary-layer flow in the vicinity of separation. We have shown how sensitive our flow is to changes in the upstream pressure gradient of only $\pm 4\%$ of $(\mathrm{d}p/\mathrm{d}x)_{max}$. If the streamwise pressure input is not precise, it will be impossible to reproduce experimental results accurately, regardless of the quality of the computational method used. On the other hand, the success of inverse methods (where δ_1 is an imput) is not surprising, since figure 3 shows that δ_1 is very sensitive to the upstream pressure gradient and in some sense already contains a fair bit of information about the 'state' of the boundary layer. A good test of the merit of a computational

technique for separating flows is its ability to reproduce the $\overline{u'^2}$ behaviour of figure 10, especially the near-wall plateau in case 3.

The authors, especially P. D., thank the Deutsche Forschungsgemeinschaft for the financial support of this investigation and appreciate the discussions with their colleagues at the Hermann-Föttinger-Institute. Special thanks are due to M. Kalter for taking some of the measurements and to Dr A. Alving for the intensive and fruitful discussion of the manuscript.

REFERENCES

ANDREOPOULOS, J., DURST, F., ZARIC, Z. & JOVANOVIC, J. 1984 Influence of Reynolds number on characteristics of turbulent wall boundary layers. *Exps Fluids* **2**, 7–16.

COLES, D. 1956 The law of the wake in the turbulent boundary layer. *J. Fluid Mech.* **1**, 191–226.

DENGEL, P. 1989 Über die Struktur und Sensibilität einer inkompressiblen turbulenten Grenzschicht am Rande der Ablösung. Eingereicht als Dissertation am FB 9 der Technischen Universität Berlin.

DENGEL, P. & FERNHOLZ, H. H. 1989 Generation of and measurements in a turbulent boundary layer with zero skin friction. *Proc. 2nd European Turbulence Conf., Berlin.* Springer.

DENGEL, P., FERNHOLZ, H. H. & HESS, M. 1987 Skin-friction measurements in two- and three-dimensional highly turbulent flows with separation. *Proc. 1st European Turbulence Conf., Lyon.* Springer.

DENGEL, P., FERNHOLZ, H. H. & VAGT, J.-D. 1982 Turbulent and mean flow measurements in an incompressible axisymmetric boundary layer with separation. *Proc. 3rd Int. Symp. on Turbulent Shear Flows. Davies* (ed. L. J. S. Bradbury *et al.*). Springer.

EAST, L. F., NASH, C. R., SAWYER, W. G. 1979 An investigation of the structure of equilibrium turbulent boundary layers. *RAE Tech. Rep.* 79040.

FERNHOLZ, H. H. 1966 Eine grenzschichttheoretische Untersuchung optimaler Unterschalldiffusoren. *Ing.-Arch.* **35**, 192–201.

FERNHOLZ, H. H. 1968 Experimentelle Untersuchung einer inkompressiblen turbulenten Grenzschicht mit Wandreibung nahe Null an einem längsangeströmten Kreiszylinder. *Z. Flugwiss.* **16**, 402–406.

FERNHOLZ, H. H. & VAGT, J.-D. 1977 Measurements in an axisymmetric turbulent boundary layer with weak and strong three-dimensional disturbances. In *Structure and Mechanics of Turbulence 1.* Lecture Notes in Physics, vol. 75 (ed. H. Fiedler), pp. 222–223. Springer.

JOHANSSON, A. V. & ALFREDSSON, P. H. 1982 On the structure of turbulent channel flow. *J. Fluid Mech.* **122**, 295–314.

PATRICK, W. P. 1987 Flowfield measurements in a separated and reattached flat plate turbulent boundary layer. *NASA CR*-4052.

PERRY, A. & SCHOFIELD, W. H. 1973 Mean velocity and shear stress distributions in turbulent boundary layers. *Phys. Fluids* **16**, 2068–2074.

PRANDTL, L. 1935 The mechanics of viscous fluids. In *Aerodynamic Theory III* (ed. W. F. Durand), pp. 34–208. Springer (see also H. Schlichting, *Grenzschichttheorie* 1964, pp. 200–202).

ROTTA, J. 1962 Turbulent boundary layers in incompressible flow. In *Progress in Aeronautical Sciences* (ed. Küchemann *et al.*), vol. 2, pp. 1–219. Pergamon.

SCHOFIELD, W. H. 1986 Two-dimensional separating turbulent boundary layers. *AIAA J.* **24**, 1611–1620.

SHILOH, K., SHIVAPRASAD, B. G. & SIMPSON, R. L. 1981 The structure of a separating turbulent boundary layer. Part 3. Transverse velocity measurements. *J. Fluid Mech.* **113**, 17–90.

SIMPSON, R. L., CHEW, Y.-T. & SHIVAPRASAD, B. G. 1981*a* The structure of a separating turbulent boundary layer. Part 1. Mean flow and Reynolds stresses. *J. Fluid Mech.* **113**, 23–51.

SIMPSON, R. L., CHEW, Y.-T. & SHIVAPRASAD, B. G. 1981*b* The structure of a separating turbulent boundary layer. Part 2. Higher-order turbulence results. *J. Fluid Mech.* **113**, 53–73.

SIMPSON, R. L., STRICKLAND, J. H. & BARR, P. W. 1977 Features of a separating turbulent boundary layer in the vicinity of separation. *J. Fluid Mech.* **79**, 553–594.

SPANGENBERG, W. G., ROWLAND, W. R. & MEASE, N. E. 1967 Measurements in a turbulent boundary layer maintained in a nearly separating condition. In *Fluid Mechanics of Internal Flow* (ed. G. Sovran), pp. 110–151. Elsevier.

STRATFORD, B. S. 1959 An experimental flow with zero skin friction throughout its region of pressure rise. *J. Fluid Mech.* **5**, 17–36.

THOMPSON, B. E. & WHITELAW, J. H. 1985 Characteristics of a trailing-edge flow with turbulent boundary-layer separation. *J. Fluid Mech.* **157**, 305–326.

VAGT, J. D. & FERNHOLZ, H. H. 1979 A discussion of probe effects and improved measuring techniques in the near wall region of an incompressible three-dimensional turbulent boundary layer. *AGARD CP* 271.

WADCOCK, A. J. 1979 Structure of the turbulent separated flow around a stalled air foil. *NASA CR*-152263.

WADCOCK, A. J. 1985 Investigation of low-speed turbulent separated flow around airfoils. *NASA CR* 177 450.